

Effect of viscoelasticity on inversion in axial deformation and on the volume of pressurized thin-walled tubes

Zdeněk Petřivý¹, Lukáš Horný^{1#}

¹Czech Technical University in Prague, Faculty of Mechanical Engineering, Technická 4, Prague, 160 00, Czech Republic

[#]Corresponding author: Lukáš Horný, lukas.horny@fs.cvut.cz

Abstract. Axial prestretching can significantly affect the mechanical response of an inflated tube. This phenomenon is known, for example in the biomechanics of the cardiovascular system, where arteries, if excised from a body, manifest non-negligible shortening. Previous studies have shown that axially prestretched tubes are more easily distensible by internal pressure than their non-prestretched counterparts. It has even been found that, in the case of the material described by the Gent strain energy density function, the volume attained by a tube at a given internal pressure can be maximized by the initial elongation of the tube to the prestretch point referred to as inversion axial prestretching. However, to the best of our knowledge, all studies dealing so far with the effect of axial prestretching on the mechanical response of a pressurized tube have assumed elastic behavior. Nevertheless, soft tissues as well as elastomer materials are always more or less viscoelastic. The present study shifts our attention from purely theoretical elastic models to a more realistic assumption of viscoelastic behavior, which is modeled by means of the Quasilinear Theory of Viscoelasticity (QLV). The adopted model assumes the elastic part of the material response to be given by the Gent model. Results suggest that the viscoelastic tube loses the property of inversion in axial deformation but can still preserve the potential to optimize the inflation volume by means of axial prestretching. This result can be helpful in designing elastomer pipelines and pumps, as well as contributing to the understanding of the principals of blood circulation physiology.

Keywords: Axial prestretching; Gent model; Hyperelasticity; Pressure; Thin-walled tube; Viscoelasticity.

1. Introduction

Axial prestretching of a cylindrical tube is a mechanical phenomenon which is known from the anatomy of the blood circulation of vertebrates (Bergel, 1961; Humphrey, 2002; Horný et al., 2014). Their arteries grow longitudinally prestretched, this is confirmed in autopsy when a segment of artery is excised from the body (Han and Fung, 1995; Horny et al., 2011; Horny et al., 2014b; Horný et al., 2017; Kamenskiy et al., 2016). When the segment is cut out, it retracts and the ratio of *in situ* to *ex situ* length is referred to as the axial prestretch. Although this phenomenon had been known about for over 100 years (Fuchs, 1900), it is only in recent decades that its mechanical consequences have been studied in detail (Horný et al., 2014, Patel and Fry, 1966; Dobrin and Doyle, 1970; Dobrin et al., 1990; Van Loon et al., 1977; Weizsäcker et al., 1983; Brossollet and Vito, 1995; Humphrey et al., 2009; Ferruzzi et al., 2018).

Ex vivo inflation experiments showed that when a cylindrical segment of an artery is pressurized at a constant length, the force necessary to hold this length constant decreases during pressure loading. On the other hand, when an artery is significantly prestretched in an axial direction and pressurization follows, the force keeping a constant length increases during the inflation (Dobrin et al., 1990;

Weizsäcker et al., 1983; Brossollet and Vito, 1995; Dobrin, 1986; Takamizawa and Hayashi, 1987). When the approach to the inflation experiment is changed from constant length to constant prestretching force (imagine for instance a weight of constant mass hanging on the lower plug of a vertically oriented tube) one also finds that pre-elongation has a significant effect on the axial response of the tube. Experiments showed that arteries inflated without axial prestretch, or when a small magnitude of prestretch is applied, elongate, whereas arteries pressurized under significant axial prestretching shorten (Ogden and Schulze-Bauer, 2000; Schulze-Bauer et al., 2003; Sommer et al., 2010; Sommer et al., 2018; Kratochvíl et al., 2020).

This suggests that there is a certain value of initial axial deformation at which subsequent pressurization will cause no change in the tube length, as well as no change to the force necessary to keep this length. This is an idealized case in which the pressure–axial stretch curve is a line perpendicular to the axial stretch axis and perfectly separates the pressure–elongation responses from the pressure–shortening responses of the tube. Thus it can be understood as an inversion in axial response; see Figure 1 which demonstrates this situation. The specific value of the axial prestretch, which in the following is denoted λ_z^{inv} , is usually referred to as the inversion stretch or inversion point (Ogden and Schulze-Bauer, 2000; Schulze-Bauer et al., 2003; Sommer et al., 2010; Sommer et al., 2018; Horný and Petřivý, 2020; Horgan and Saccomandi, 2003; Ogden and Saccomandi, 2007).

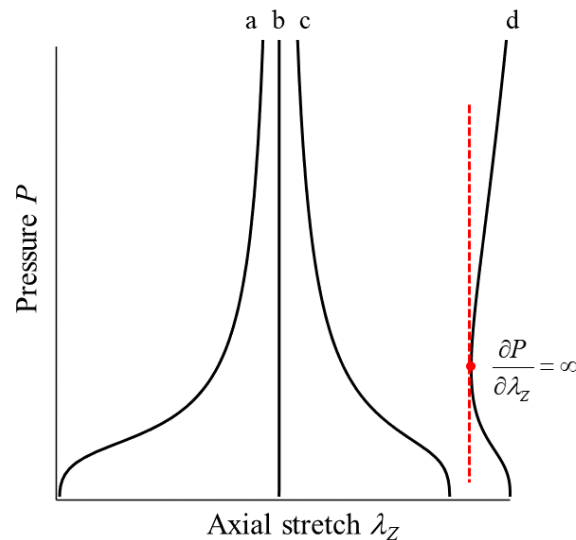


Figure 1. Axial response of a cylindrical tube to internal pressure. Pressure-induced elongation – a, perfect inversion separating elongation and shortening (inversion line, global inversion) – b, pressure-induced shortening – c, non-monotonous response with local inversion – d.

In arterial biomechanics, a generally accepted hypothesis states that the physiological axial deformation of arteries, which is in fact immeasurable *in vivo*, just corresponds to a state in which the prestretching force is independent of applied pressure, which occurs just at the inversion point (Van Loon et al., 1977; Brossollet and Vito, 1995; Humphrey et al., 2009).

A consequence of axial prestretching, which has been emphasized only recently, is that longitudinally prestretched tubes can exhibit a more compliant pressure–circumferential stretch response than non-prestretched tubes (Horný et al., 2014; Horný and Petřivý, 2020; Horný and Netušil, 2016). This means that axial prestretching makes the tube capable of a higher radial distension at a given pressure than its non-prestretched counterpart. This property could be another physical principle that contributed to the evolution of axial prestretching in blood vessels.

Horný and Netušil (2016) discussed in detail what the source is of increased distensibility of the prestretched tubes. They arrived at the conclusion that it is a nonlinearity. Linearly elastic tubes at infinitesimal strains do not show any increase in the distensibility when axial prestretching is applied, whereas the formulation of the thin-walled tube inflation within the second order theory of linear elasticity (linear material with infinitesimal deformations but with large displacements being considered) showed an increase in the distensibility of the pressurized tube. The effect of the prestretching on the mechanical response of the tube was amplified when a true hyperelastic formulation was applied (Horný and Netušil, 2016).

In our recent paper (Horný and Petřivý, 2020), it was shown that the inflation of the tube at the inversion axial stretch is accompanied by another interesting property, namely that the tube attains maximum internal volume. This means that at a given pressure, the tube accommodates the maximum volume of pressurizing media, if it is pressurized at the inversion stretch. This result gives rise to the hypothesis that our bodies evolved in such a way that the aorta is prestretched to a state ensuring the transport of the maximal volume of blood during one heart cycle.

It is shown in (Horný and Petřivý, 2020) that perfect axial inversion and maximal volume are coinciding phenomena and that closed thin-walled tubes made from materials corresponding to Mooney-Rivlin and Gent strain energy density have these properties. It is in contrast to the Holzapfel-Gasser-Ogden (HGO) strain energy density function, which is frequently used in arterial mechanics. It does not exhibit perfect inversion; a situation in which a tube axially prestretched by constant force exhibits a constant axial deformation during the entire pressurization process. Nevertheless, the pressurization curves of an HGO tube exhibit points where the derivative of the pressure with respect to the axial stretch does not exist. This means that the axial response of the tube is not monotonous during pressurization. At a certain value of the pressure, pressure-induced shortening of the tube changes to pressure-induced elongation and points, where this happens, have tangents which are perpendicular to the horizontal axis of the graph, see Figure 1. At these points, which can be understood as local inversions, the maximal inflation volume is attained (Horný and Petřivý, 2020).

To the best of our knowledge, all works so far which have studied inversion in the axial deformation of a pressurized tube are based on the assumption of elastic behavior. It is, however, well-known that elastomer materials as well as biological tissues, ordinary candidates for the application of our results, are more or less viscoelastic. Hence, a question which naturally arises is as to whether a viscoelastic tube will also exhibit inversion axial stretch and if the internal volume of a viscoelastic tube can be optimized by means of axial prestretching. This is the main objective of our study.

Since our primary objective is to show the differences induced by a transition from elastic to viscoelastic material behavior, at first, equations describing the elastic case are briefly presented. Subsequently, the Quasi-Linear theory of Viscoelasticity (QLV) is used to introduce the viscoelastic material model and the problem of an axially prestretched thin-walled tube loaded by internal pressure is formulated. QLV is based on a multiplicative decomposition of viscous and elastic effects, and enables direct incorporation of the Gent's strain energy density function into the viscoelastic formulation. Differences between elastic and viscoelastic cases are demonstrated by a numerical solution to the problem of the inflation and extension of a thin cylindrical shell. Both cases, a closed tube prestretched by axial force which is constant during pressurization and an open tube held at constant length during pressurization, are studied. It is shown that viscoelasticity leads to a loss of perfect axial inversion in the Gent tube but axial prestretch maximizing the inflation volume still exists.

2. Modeling of the thin-walled tube inflation and extension

The present paper can be understood as a continuation of (Horný and Netušil, 2016) and (Horný and Petřivý, 2020), where the effect of axial prestretching on the inflation of nonlinearly elastic thin-walled

tubes has been studied. Each of these papers uses a different derivation of equations describing the thin-walled tube inflation problem. The derivation used in (Horný and Petřivý, 2020) approaches the thin-walled approximation using the Mean Value theorem applied to a general, thick-walled tube equilibrium. The method used in (Horný and Netušil, 2016) is based on the thin shell theory and uses the free body diagram of a cylindrical pressure vessel. Although the former is perhaps mathematically more rigorous, the latter will be adopted here particularly due to its straightforward extension to a viscoelastic case.

2.1 Elastic tube

Kinematics. Polar cylindrical coordinates will be used within the entire study. Consider a long thin-walled cylindrical tube, which in the reference configuration has middle radius R , thickness H , and length L . Assume that during loading, the tube undergoes uniform inflation and extension such that it preserves its cylindrical shape and that it does not undergo shear deformation. In such a case, the motion of a material particle located originally at (R, Θ, Z) is described by the equations (1).

$$r = \lambda_\Theta R \quad \theta = \Theta \quad z = \lambda_Z Z \quad (1)$$

Here (r, θ, z) are deformed coordinates of the particle. Since the tube is thin-walled and inflates and extends uniformly, λ_Θ expresses its circumferential and λ_Z its axial stretch ratio. The same arguments lead us to $h = \lambda_R H$ as an expression for deformed thickness h where λ_R denotes the radial stretch ratio. The deformation gradient \mathbf{F} thus has the form $\mathbf{F} = \text{diag}[\lambda_R, \lambda_\Theta, \lambda_Z]$. The right Cauchy-Green deformation tensor \mathbf{C} is given as $\mathbf{C} = \mathbf{F}^T \mathbf{F} = \text{diag}[\lambda_R^2, \lambda_\Theta^2, \lambda_Z^2]$. Principal invariants of \mathbf{C} can be expressed by means of (2).

$$I_1 = \text{tr}(\mathbf{C}) \quad I_2 = \frac{1}{2} \left(\text{tr}^2(\mathbf{C}) - \text{tr}(\mathbf{C}^2) \right) \quad I_3 = \det(\mathbf{C}) \quad (2)$$

Macromolecular materials, like elastomers and soft tissues, are frequently modeled as incompressible (Gent, 1996; Marckmann and Verron, 2006; Fung, 1981; Holzapfel, 2000). This assumption will also be adopted in our study, thus only isochoric deformations are considered. In such a case $I_3 = 1$ holds.

The internal volume accommodated in the uniformly inflated and extended thin-walled cylindrical tube can be approximated by $\pi r^2 l$. Dividing this expression by the reference internal volume $\pi R^2 L$ and substituting from (1), one obtains (3) which expresses the normalized internal volume of the tube v achieved during its pressurization.

$$v = \lambda_\Theta^2 \lambda_Z \quad (3)$$

Constitutive equation. The material of the tube is considered to be hyperelastic. Thus there is the strain energy density function W , which plays a role of the elastic potential. In such a case, Cauchy stress $\boldsymbol{\sigma}$ can be obtained by means of the differentiation of W with respect to \mathbf{F} as expressed in (4). Here \mathbf{I} is the second order unit tensor and p is a multiplier introduced due to the incompressibility constraint and has to be determined with the help of a boundary condition.

$$\boldsymbol{\sigma} = \frac{\partial W}{\partial \mathbf{F}} \mathbf{F}^T - p \mathbf{I} \quad (4)$$

The specific form of W used in our study is the Gent's strain energy density function. This model was introduced by A.N. Gent in (Gent, 1996). It has been shown that the Gent model is suitable for use in the elastic description of various elastomers (Gent, 1996; Horgan and Saccomandi, 2002b; Kanner and Horgan, 2007; Marckmann and Verron, 2006; Zhou et al., 2018), and can also be used in biomechanics

to model a response of soft tissues when an assumption of material isotropy is adequate (Horgan and Saccomandi, 2003; Horny et al., 2013; Mihai et al., 2015; Zhang et al., 2016; Mangan and Destrade, 2015). The equation (5) expresses its concrete mathematical form.

$$W = -\frac{\mu J_m}{2} \ln \left(1 - \frac{I_1 - 3}{J_m} \right) \quad (5)$$

In (5), μ is a stress-like material parameter corresponding at infinitesimal strains to the shear modulus. J_m is a dimensionless parameter modulating the strain stiffening of the material. Gent's material model belongs to the class of so-called limiting chain extensibility models, which means that admissible deformations are restricted to a certain subset in the space of all deformations. It is clear from (5) that an admissible deformation has to satisfy $I_1 < J_m + 3$. Due to this fact, stress-strain curves obtained for Gent's material exhibit significant stiffening when I_1 approaches $J_m + 3$. The equations (6) express specific stress-strain relations as are obtained when (5) is substituted into (4).

$$\sigma_{rr} = \mu J_m \frac{\lambda_R^2}{J_m + 3 - I_1} - p \quad \sigma_{\theta\theta} = \mu J_m \frac{\lambda_\Theta^2}{J_m + 3 - I_1} - p \quad \sigma_{zz} = \mu J_m \frac{\lambda_Z^2}{J_m + 3 - I_1} - p \quad (6)$$

Equilibrium equations. Figure 2 depicts the pressurization of an axially prestretched tube. Two cases are technically important. The left panel shows the tube which is initially deformed to the stretch ratio λ_Z^{ini} by elongating the length of the tube from L to $l = \lambda_Z^{ini} L$. This is considered to be kinematical loading. This loading induces some reaction force F_{red} (not depicted in the left panel). Subsequently, in the longitudinally prestretched state, the tube is pressurized by internal pressure P . The bond holds the tube at constant length during pressurization, whereas F_{red} induced by this bond varies. This is the first case. The right panel shows pressurization at a constant prestretching force F_{red} . In this second case, axial prestretching is achieved by the initial application of F_{red} , which could be realized, for example, by hanging some weight of constant mass. The application of F_{red} at $P = 0$ induces axial prestretch λ_Z^{ini} . Subsequently, the tube is loaded by internal pressure P . Since the tube is not held by a kinematical bond in the axial direction, pressurization can cause a change of the current value of λ_Z .

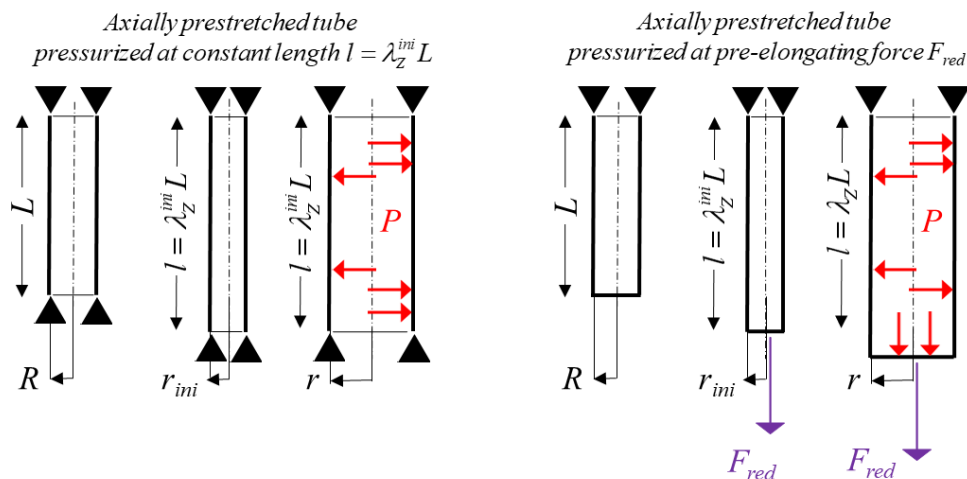


Figure 2. Open versus closed tube. The sketch elucidates the difference between the pressurization of the open tube at a constant length achieved during initial axial prestretching (left panel), and the pressurization of the closed tube under a constant prestretching force F_{red} (right panel).

Since our model is based on the thin-walled tube, it is assumed that external loading to the tube is balanced by membrane stresses. In such a case, the balance equations have the form of (7).

$$\sigma_{rr} = 0 \quad \sigma_{\theta\theta} = \frac{rP}{h} \quad \sigma_{zz} = \delta \frac{rP}{2h} + \frac{F_{red}}{2\pi rh} \quad (7)$$

The equation (7)₁ is a consequence of the thin-wall assumption. (7)₂ corresponds to the Laplace law in the circular cylindrical shell. Finally, (7)₃ expresses that there are two sources of the axial loading carried by the tube wall. The first is the contribution made by pressure P acting on the closed end of the tube, and the second is due to the prestretching achieved by F_{red} . Factor δ switches between closed and open tube formulation; $\delta = 1$ corresponds to the closed tube, whereas $\delta = 0$ applies for the tube which does not carry an axial force induced by the pressure acting on the cover.

Final system of equations. Governing equations for the inflation and extension of the thin-walled tube are obtained when the left sides in (7) are substituted from (6) and (1) is used on the right sides of (6). Finally λ_R is substituted from the incompressibility condition written as $\lambda_R = (\lambda_\theta \lambda_z)^{-1}$. (7)₁ is used to determine p , which is then substituted into (7)₂ a (7)₃. These algebraic manipulations result in the system expressed in (8) where denotation $\bar{I}_1 = (\lambda_\theta \lambda_z)^{-2} + \lambda_\theta^2 + \lambda_z^2$ is used.

$$\frac{\lambda_\theta^2}{J_m + 3 - \bar{I}_1} - \frac{1}{J_m + 3 - \bar{I}_1} \frac{1}{\lambda_\theta^2 \lambda_z^2} = \frac{RP}{H \mu J_m} \lambda_\theta^2 \lambda_z \quad (8)_1$$

$$\frac{\lambda_z^2}{J_m + 3 - \bar{I}_1} - \frac{1}{J_m + 3 - \bar{I}_1} \frac{1}{\lambda_\theta^2 \lambda_z^2} = \delta \frac{RP}{2H \mu J_m} \lambda_\theta^2 \lambda_z + \frac{F_{red}}{2\pi RH \mu J_m} \lambda_z \quad (8)_2$$

The system (8)₁ a (8)₂ describes the mechanical behavior of the tube. When tube reference geometry $\{R, H\}$ and material parameters $\{\mu, J_m\}$ are known, these two equations can be used to determine two unknowns from quadruplet $\{P, F_{red}, \lambda_\theta, \lambda_z\}$. The remaining pair is considered as independent variables and represents loading. In this section, the dependence on time t was not explicitly indicated because in the elasticity, loading history does not enter into the constitutive equation and the mechanical response depends only on the present state.

2.2 Viscoelastic tube

Kinematics. The mechanical response of viscoelastic materials depends on the deformation history. It follows that in addition to the current instant of time denoted as t , in which one wants to determine the stress state, time denoted as s , used to account for past deformation states, is introduced. Deformation gradient \mathbf{F} is then given by (9).

$$\mathbf{F}(s) = \begin{cases} \mathbf{I} & s \in (-\infty, 0) \\ \text{diag}[\lambda_R(s), \lambda_\theta(s), \lambda_z(s)] & s \in [0, t] \end{cases} \quad (9)$$

The kinematics of the inflation and extension of the tube is considered in the same form as in the elastic case (1). Thus we again assume that the tube preserves its shape of a circular cylinder and that no shear strain is considered. Dependence on time will be explicitly highlighted only if there is a risk of confusion between t and s .

Constitutive equation. The Quasi-Linear Theory of Viscoelasticity has been introduced by Y. C. Fung in (Fung, 1981). Its relation to the other theories of viscoelastic material behavior can be found in (Wineman, 2020), which is a part of Merodio and Ogden (2020). In what follows, our theoretical considerations are restricted to the aspects necessary for studying the problem of the inflation and

extension of the thin viscoelastic tube. Readers interested in further details of the theory of viscoelasticity can consult with works covering the subject of the constitutive modeling more generally (Christensen 1982; Merodio and Rajagopal 2007; Bergström 2015; Merodio and Ogden, 2020; Jha et al., 2019; Zhang et al., 2022). Our specific approach is based on recent works by De Pascalis and co-workers (De Pascalis et al., 2014; De Pascalis et al., 2018).

QLV uses the standard Boltzmann integral formulated within the finite strain theory. The fundamental idea is that viscous effects and the effect of material nonlinearity can be separated from each other and, in fact, are assumed to be mutually independent. The general QLV constitutive equation in index notation is expressed in (10).

$$S_{IJ}(t) = \int_{-\infty}^t G_{IJKL}(t-s) \frac{\partial S_{KL}^e(s)}{\partial s} ds \quad (10)$$

S_{IJ} denotes the components of the viscoelastic second Piola-Kirchhoff stress tensor \mathbf{S} , determined at the current instant of time t , G_{IJKL} represents the reduced relaxation function which, in the most general approach can be understood as the fourth order tensor and represents viscous phenomena in the material response, and S_{KL}^e denotes components of the second Piola-Kirchhoff stress corresponding to the elastic response of the material, which is considered to be given by elastic potential W .

The second Piola-Kirchhoff stress, since it is related to the reference configuration, offers the advantage of naturally preserving objectivity when differentiation with respect to time is carried out. However, balance equations (7) are derived at the current configuration, hence they are written with the help of the Cauchy stress $\boldsymbol{\sigma}$. The transformation between \mathbf{S} and $\boldsymbol{\sigma}$ is given by (11). Here J is the volume ratio defined as $J = \det(\mathbf{F})$.

$$\mathbf{S} = J\mathbf{F}^{-1}\boldsymbol{\sigma}\mathbf{F}^{-T} \quad (11)$$

It is convenient to consider $\boldsymbol{\sigma}$ decomposed into deviatoric, $\boldsymbol{\sigma}_D = \boldsymbol{\sigma} - \frac{1}{3}\text{tr}(\boldsymbol{\sigma})\mathbf{I}$, and hydrostatic, $\boldsymbol{\sigma}_H = \frac{1}{3}\text{tr}(\boldsymbol{\sigma})\mathbf{I}$, part. The expression $\boldsymbol{\sigma} = \boldsymbol{\sigma}_D + \boldsymbol{\sigma}_H$ is transformed into a material description by means of (11). It follows that the second Piola-Kirchhoff stress can be written as decomposed into parts corresponding to deviatoric and hydrostatic Cauchy stress; $\mathbf{S} = J\mathbf{F}^{-1}\boldsymbol{\sigma}\mathbf{F}^{-T} = J\mathbf{F}^{-1}(\boldsymbol{\sigma}_D + \boldsymbol{\sigma}_H)\mathbf{F}^{-T}$. These two parts will be denoted as \mathbf{S}_D and \mathbf{S}_H as expressed in (12).

$$\mathbf{S} = \mathbf{S}_D + \mathbf{S}_H \quad \mathbf{S}_D = J\mathbf{F}^{-1}\boldsymbol{\sigma}_D\mathbf{F}^{-T} \quad \mathbf{S}_H = J\mathbf{F}^{-1}\boldsymbol{\sigma}_H\mathbf{F}^{-T} \quad (12)$$

In the present study, we restrict our attention to the isotropic reduced relaxation function. In such a case, the equation (10) can, when the deviatoric–volumetric decomposition introduced in (12) is applied to elastic \mathbf{S}^e , be written by means of (13). Here $\mathcal{D}(t)$ and $\mathcal{H}(t)$ are scalar reduced relaxation functions respectively corresponding to dilatational and hydrostatic response.

$$\mathbf{S}(t) = \int_{-\infty}^t \mathcal{D}(t-s) \frac{\partial \mathbf{S}_D^e(s)}{\partial s} ds + \int_{-\infty}^t \mathcal{H}(t-s) \frac{\partial \mathbf{S}_H^e(s)}{\partial s} ds \quad (13)$$

Viscoelastic Cauchy stress $\boldsymbol{\sigma}(t)$ is obtained from (13) by means of inversely applied transformation (11), which results in (14).

$$\boldsymbol{\sigma}(t) = J^{-1}\mathbf{F} \left(\int_{-\infty}^t \mathcal{D}(t-s) \frac{\partial \mathbf{S}_D^e(s)}{\partial s} ds \right) \mathbf{F}^T + J^{-1}\mathbf{F} \left(\int_{-\infty}^t \mathcal{H}(t-s) \frac{\partial \mathbf{S}_H^e(s)}{\partial s} ds \right) \mathbf{F}^T \quad (14)$$

Considering that all physical processes, i.e. deformation, loading and relaxation, are triggered at $t = 0$ leads to the change in the lower integration limit from $-\infty$ to 0 and to the normalization condition for reduced relaxation functions $\mathcal{D}(0) = \mathcal{H}(0) = 1$. Bearing this in mind and applying integration by parts in (14), one arrives at (15).

$$\boldsymbol{\sigma}(t) = J^{-1} \mathbf{F} \left(\mathbf{S}_D^e(t) + \int_0^t \frac{\partial \mathcal{D}(t-s)}{\partial s} \mathbf{S}_D^e(s) ds \right) \mathbf{F}^T + J^{-1} \mathbf{F} \left(\mathbf{S}_H^e(t) + \int_0^t \frac{\partial \mathcal{H}(t-s)}{\partial s} \mathbf{S}_H^e(s) ds \right) \mathbf{F}^T \quad (15)$$

As the final step, incompressibility assumption is introduced into the viscoelastic description. Here we follow the arguments introduced in (De Pascalis et al., 2014; De Pascalis et al., 2018). To be more specific, from an internal forces point of view, the incompressibility means that compressive disturbances can propagate at infinite speed. On the other hand, it implies that the relaxation time for viscose dilatational motions can be assumed to be zero. Therefore, the hydrostatic part in (15) reduces to multiplier $p(t)$ in a similar way as in incompressible elasticity.

$$J^{-1} \mathbf{F} \left(\mathbf{S}_H^e(t) + \int_0^t \frac{\partial \mathcal{H}(t-s)}{\partial s} \mathbf{S}_H^e(s) ds \right) \mathbf{F}^T \rightarrow p(t) \mathbf{I} \quad (16)$$

Thus (16) applies and when introduced into (15), it results in the final constitutive equation for viscoelastic incompressible material which is expressed in (17).

$$\boldsymbol{\sigma}(t) = J^{-1} \mathbf{F} \left(\mathbf{S}_D^e(t) + \int_0^t \frac{\partial \mathcal{D}(t-s)}{\partial s} \mathbf{S}_D^e(s) ds \right) \mathbf{F}^T - p(t) \mathbf{I} \quad (17)$$

The elastic second Piola-Kirchhoff stress \mathbf{S}_D^e corresponding to the deviatoric part of the elastic Cauchy stress $\boldsymbol{\sigma}_D^e$, which appears in (17) can be obtained in various ways from the general elastic constitutive equation (18). In (18), the standard denotation $W_k = \partial W / \partial I_k$, where $k = 1, 2, 3$, is used, and \mathbf{b} denotes the left Cauchy-Green strain tensor, which is defined as $\mathbf{b} = \mathbf{F} \mathbf{F}^T$.

$$\boldsymbol{\sigma}^e = 2J^{-1} \left[(I_2 W_2 + I_3 W_3) \mathbf{I} + W_1 \mathbf{b} - I_3 W_2 \mathbf{b}^{-1} \right] \quad (18)$$

One formula, adopted from (De Pascalis et al., 2014), is obtained by applying deviatoric–volumetric decomposition on (18), considering that $I_3 = 1$ holds for incompressible materials, and applying transformation (11) to the decomposition result. The final expression of \mathbf{S}_D^e is given in (19).

$$\mathbf{S}_D^e = 2 \left[W_1 \mathbf{I} + \frac{1}{3} (I_2 W_2 - I_1 W_1) \mathbf{C}^{-1} - W_2 \mathbf{C}^{-2} \right] \quad (19)$$

The viscoelastic constitutive model has to be completed with a specification of W and \mathcal{D} . In order to easily determine the effect of viscoelasticity on the inflation response, the Gent model defined in (5) will be used. For the sake of easy comparison with the elastic case, a one-term relaxation function in the form given by (20) is considered in our study. Here μ has the same meaning as in (5), μ_∞ is the long-time infinitesimal shear modulus, and τ is the relaxation time.

$$\mathcal{D}(t) = \frac{\mu_\infty}{\mu} + \left(1 - \frac{\mu_\infty}{\mu} \right) e^{-\frac{t}{\tau}} \quad (20)$$

The particular form of the stress-strain relationship, which is obtained when the Gent strain energy density function (5) is substituted into (19) and then the result is simultaneously substituted with (20)

into (17), is explicitly written in (21). These equations express our viscoelastic constitutive model and, in what follows, will also be referred to as QLV-Gent.

$$\sigma_{rr}(t) = \mu J_m \frac{3\lambda_R^2(t) - I_1(t)}{3(J_m + 3 - I_1(t))} - \mu J_m \lambda_R^2(t) \int_0^t \mathcal{D}'(t-s) \frac{3\lambda_R^2(s) - I_1(s)}{3\lambda_R^2(s)(J_m + 3 - I_1(s))} ds - p(t) \quad (21)_1$$

$$\sigma_{\theta\theta}(t) = \mu J_m \frac{3\lambda_\Theta^2(t) - I_1(t)}{3(J_m + 3 - I_1(t))} - \mu J_m \lambda_\Theta^2(t) \int_0^t \mathcal{D}'(t-s) \frac{3\lambda_\Theta^2(s) - I_1(s)}{3\lambda_\Theta^2(s)(J_m + 3 - I_1(s))} ds - p(t) \quad (21)_2$$

$$\sigma_{zz}(t) = \mu J_m \frac{3\lambda_Z^2(t) - I_1(t)}{3(J_m + 3 - I_1(t))} - \mu J_m \lambda_Z^2(t) \int_0^t \mathcal{D}'(t-s) \frac{3\lambda_Z^2(s) - I_1(s)}{3\lambda_Z^2(s)(J_m + 3 - I_1(s))} ds - p(t) \quad (21)_3$$

$I_1(x)$, where $x = s, t$, appearing in (21), denotes $I_1(x) = \lambda_R^2(x) + \lambda_\Theta^2(x) + \lambda_Z^2(x)$. In order to abbreviate the above mentioned expressions, the denotation $\mathcal{D}'(t) = \partial \mathcal{D}(t)/\partial t$ was introduced and the specific form of the derivative is given by (22).

$$\mathcal{D}'(t-s) = -\tau^{-1} \left(1 - \frac{\mu_\infty}{\mu} \right) e^{-\frac{t-s}{\tau}} \quad (22)$$

Equilibrium equations. The geometry of the studied tube and its loading are the same in the viscoelastic case as in the elastic one. The only difference that occurs here is the different constitutive model. Thus the equilibrium equations for a thin cylindrical shell expressed in (7) are easily modified into the viscoelastic case when the explicit dependence on time of the left sides, i.e. $\sigma_{rr}(t)$, $\sigma_{\theta\theta}(t)$, and $\sigma_{zz}(t)$, is considered. In a similar way, one can also indicate an explicit dependence on time on the right sides of the equations.

Final system of equations. The governing equations for the inflation and extension of the thin-walled viscoelastic tube are again obtained when the left sides in (7) are substituted with the stress components determined from the constitutive equations (21). At the same time, the right sides of (7) are substituted with (1) bearing in mind that a dependence on time t is considered. In the final system, λ_R is substituted from the incompressibility condition written as $\lambda_R(t) = (\lambda_\Theta(t)\lambda_Z(t))^{-1}$, which in integrands is modified to a dependence on s . Similarly to the elastic case, (7)₁ is used to find $p(t)$, which is then substituted into (7)₂ a (7)₃. The resulting system then describes the mechanical behavior of the viscoelastic tube and the explicit expressions are given in (23).

$$\frac{\lambda_\Theta^4(t)\lambda_Z^2(t) - 1}{\lambda_\Theta^2(t)\lambda_Z^2(t)(J_m + 3 - \bar{I}_1(t))} - \frac{\lambda_\Theta^2(t)}{3} \int_0^t \mathcal{D}'(t-s) \frac{2\lambda_\Theta^2(s) - \lambda_Z^2(s) - \lambda_\Theta^{-2}(s)\lambda_Z^{-2}(s)}{\lambda_\Theta^2(s)(J_m + 3 - \bar{I}_1(s))} ds \quad (23)_1$$

$$+ \frac{1}{3\lambda_\Theta^2(t)\lambda_Z^2(t)} \int_0^t \mathcal{D}'(t-s) \frac{2 - \lambda_\Theta^4(s)\lambda_Z^2(s) - \lambda_\Theta^2(s)\lambda_Z^4(s)}{(J_m + 3 - \bar{I}_1(s))} ds = \frac{P(t)R\lambda_\Theta^2(t)\lambda_Z(t)}{\mu J_m H}$$

$$\frac{\lambda_\Theta^2(t)\lambda_Z^4(t) - 1}{\lambda_\Theta^2(t)\lambda_Z^2(t)(J_m + 3 - \bar{I}_1(t))} - \frac{\lambda_Z^2(t)}{3} \int_0^t \mathcal{D}'(t-s) \frac{2\lambda_Z^2(s) - \lambda_\Theta^2(s) - \lambda_\Theta^{-2}(s)\lambda_Z^{-2}(s)}{\lambda_\Theta^2(s)(J_m + 3 - \bar{I}_1(s))} ds \quad (23)_2$$

$$+ \frac{1}{3\lambda_\Theta^2(t)\lambda_Z^2(t)} \int_0^t \mathcal{D}'(t-s) \frac{2 - \lambda_\Theta^4(s)\lambda_Z^2(s) - \lambda_\Theta^2(s)\lambda_Z^4(s)}{(J_m + 3 - \bar{I}_1(s))} ds = \delta \frac{P(t)R\lambda_\Theta^2(t)\lambda_Z(t)}{2\mu J_m H} + \frac{F_{red}(t)\lambda_Z(t)}{2\pi R H \mu J_m}$$

2.3 Inversion in axial deformation

As explained in the Introduction, we are primarily focused on the axial response of a pressurized tube. Figure 1 shows how the axial deformation can vary during pressurization. One can distinguish three

characteristics of monotonous response: $\lambda_z = \lambda_z(P)$ is increasing function (a), $\lambda_z = \lambda_z(P)$ is constant function (referred to as *inversion line*, b), and $\lambda_z = \lambda_z(P)$ is decreasing function (c). These kinds of response were studied in detail, for example in (Brossollet and Vito, 1995; Humphrey et al., 2009; Ogden and Schulze-Bauer, 2000; Horný and Petřivý, 2020; Horgan and Saccomandi, 2003; Ogden and Saccomandi, 2007; Horný and Netušil, 2016). In particular, axial inversion as a highly interesting phenomenon was analyzed, and the necessary condition that \hat{W} has to satisfy in order to exhibit an inversion line in the axial response of the pressurized tube, has been presented in (Ogden and Schulze-Bauer, 2000; Horný and Petřivý, 2020; Horgan and Saccomandi, 2003; Ogden and Saccomandi, 2007). The condition can be written in the form (24).

$$\lambda_\Theta \frac{\partial^2 \hat{W}}{\partial \lambda_\Theta^2} + \frac{\partial \hat{W}}{\partial \lambda_\Theta} - 2\lambda_z \frac{\partial^2 \hat{W}}{\partial \lambda_\Theta \partial \lambda_z} = 0 \quad (24)$$

Here \hat{W} is the strain energy density function, with the radial stretch substituted by means of the incompressibility condition, $\hat{W} = W(\lambda_r(\lambda_\Theta, \lambda_z), \lambda_\Theta, \lambda_z)$. All steps necessary to derive this equation can be found, for example in (Horný and Petřivý, 2020), and we will not repeat them here. The key point of the derivation is to realize that due to the relationship between pressure and circumferential stretch, the axial inversion is also exhibited in the λ_z - λ_Θ relationship. This leads to the condition $\partial \lambda_z / \partial \lambda_\Theta = 0$. One can employ the implicit function theorem to create this derivative, $\partial \lambda_z / \partial \lambda_\Theta = -(\partial F / \partial \lambda_\Theta) / (\partial F / \partial \lambda_z)$, and F_{red} can be used to express $F(\lambda_\Theta, \lambda_z)$.

In our previous paper (Horný and Petřivý, 2020), a similar approach was adopted to express the condition for W under which the thin-walled tube would exhibit maximal internal volume during inflation. In such a problem, we are asking at which axial prestretching the tube pressurized by a given pressure P will attain its maximal internal volume v ? Such a question is of clear technical importance in engineering design and in the physiology of blood circulation. The response is again obtained by means of the implicit function theorem, $\partial v / \partial \lambda_z = -(\partial F / \partial \lambda_z) / (\partial F / \partial v) = 0$, but now with the help of P as $F(v, \lambda_z)$. Nevertheless, as the first step, one has to employ (3) to substitute λ_Θ by v in the equations describing the inflation and extension of the tube.

It has been shown in (Horný and Petřivý, 2020) that Gent's strain energy density function (5) is an example of the material model that exhibits axial inversion in the inflation of the tube and the maximization of the internal volume by means of axial prestretching. Both volume maximization and axial inversion occur at the same prestretch λ_z^{ini} which is given by the expression $\lambda_z^{ini} = \sqrt{1 + 1/3 J_m}$. In contrast to the elastic case, the hereditary integrals in (23) make a similar approach only barely feasible in the case of viscoelastic material. For this reason, our examination of the mechanical response of a viscoelastic tube will be based on the numerical solution to the equations (23).

3. Solution procedure

The comparison between the elastic and viscoelastic mechanical response of the tube is carried out with the help of computational simulations. Details of the simulations depend on which kind of material is used (elastic vs. viscoelastic) and on the form of the axial boundary condition (constant length vs. constant prestretching force, cf. Fig. 2). Reference geometry $\{R, H\}$ and material parameters $\{\mu, J_m, \mu_\infty, \tau\}$ are considered to be given quantities. Our simulations will show how the tube responds to the pressurization, hence P is understood as a known variable. The specific values of the longitudinal prestretching used in our study are $\lambda_z^{ini} \in \{1, 1.207, 1.311, 1.414, 1.518, 1.621, 1.828\}$.

Elastic case – closed tube. A prediction of the inflation-extension response is obtained in two steps. First, the axial prestretch of the tube is induced by assigning $\lambda_z = \lambda_z^{ini}$ at zero pressure. By solving (8)₁ and (8)₂, F_{red} and λ_Θ^{ini} are found. In the second step, the equations (8)₁ and (8)₂ are used to calculate λ_z

and λ_Θ for a given loading pressure P and F_{red} which corresponds to the chosen λ_Z^{ini} . In all these steps $\delta = 1$ is used.

Elastic case – open tube. In this case, the simulation is performed with a one step procedure. The chosen value of the axial prestretch, λ_Z^{ini} , is substituted into (8)₁ and (8)₂ and because the loading pressure is considered to be assigned, the remaining unknowns, λ_Θ and F_{red} , are obtained from the equations (8). $\delta = 0$ holds in this case because, if the length of the tube is constant, there must be some bond which holds the tube at its ends. This bond prevents the force generated by the pressure acting on a cover to be transferred to the tube wall.

Viscoelastic case. As has been mentioned in the derivation of the constitutive model, relaxation processes are considered to have been triggered when $t = 0$. Instead of considering a purely theoretical jump loading to induce axial prestretch in the tube, which would correspond to the way in which a classical relaxation experiment is usually explained in school classes, a more realistic approach, which can be carried out in a laboratory, taking into consideration certain time interval necessary to induce the prestretching, is adopted.

Viscoelastic case – closed tube. This case corresponds to a constant prestretching force F_{red} . At first, a particular value of λ_Z^{ini} is chosen. In the first loading step, the prestretching force is linearly increased from $F_{red} = 0$ at $t = 0$ to the value which corresponds to F_{red} obtained from an elastic solution for considered λ_Z^{ini} . This prestretching period, in which F_{red} consecutively increases, lasts 1 s. The pressure is zero during the initial axial stretching and the solution of (23)₁ and (23)₂ gives $\lambda_Z(t)$ and $\lambda_\Theta(t)$. When the final value of F_{red} is reached, pressurization follows. In this second loading step, the pressure linearly increases and the loading process spans 50 s. F_{red} and $P(t)$ are substituted into (23)₁ and (23)₂ and $\lambda_Z(t)$ and $\lambda_\Theta(t)$ are obtained by means of the numerical solution.

Viscoelastic case – open tube. This case corresponds to the constant axial deformation $\lambda_Z = \lambda_Z^{ini}$ during tube pressurization. However, to achieve axial prestretching in a realistic manner, instead of a jump loading, a prestretching step is introduced. Thus, similarly to the closed tube, the first loading step consists in the linear increase of $\lambda_Z(t)$ from $\lambda_Z = 1$ at $t = 0$ to $\lambda_Z = \lambda_Z^{ini}$ at $t = 1$ s. The pressurization period follows, in which P linearly increases. The pressurization again lasts 50 s.

Technical details of the computations. Specific values of material parameters and reference geometry were considered as described in Table 1. In fact, as is clear from the systems (8) and (23), the equations can be easily modified to the dimensionless form, hence only H/R , J_m , μ_∞ , and τ are technically important. All calculations were carried out with the help of computer algebra software Maple 2020. Integrals in (23) were integrated numerically and the results obtained in time t were substituted as the history in the $t + \Delta$ step. To show how a viscoelastic response depends on the pressurization speed, the inflation was conducted twice. The first, which is understood as the *slow loading* pressurization, lasted 50 s as described above. In the second, understood as the *rapid loading*, all parameters were the same as explained above, but the linear pressurization was shortened to last only 2 seconds. In the slow loading, the uniform time increment $\Delta = 0.2$ s was used, and in the rapid loading, the increment was $\Delta = 0.002$ s.

Table1. Parameter values used in the simulations.

J_m	μ	μ_∞	τ	R	H
3	1	0.5	2	1	0.05

4. Results and Discussion

Our simulations show the role played by axial prestretching in the mechanical response of a pressurized thin-walled tube. Since realistic macromolecular materials are more or less viscoelastic, our simulations involved one representation of viscoelastic behavior. Figures 3 – 6 display specific numerical results and elastic and viscoelastic responses are compared within them. The results presented in Fig. 3 and 4 correspond to the closed tube, whereas the results for the open tube formulation are displayed in Fig. 5 and 6.

Figures 3 – 6 are all arranged in the same way. From the upper left to the lower right panel, they consecutively show $F_{red}(t)$, and $P(t)$ applied in the loading, and $P-\lambda_\Theta$, $P-\lambda_Z$, and $v-P$ obtained as the results of the simulations. Colors are used to indicate the value of the axial prestretching applied in the loading. Dotted curves correspond to the results of the elastic formulation whereas solid curves are used for viscoelastic behavior. With regard to the loading velocity, note the differences in $F_{red}(t)$ and $P(t)$ on Fig. 3 and 5, which correspond to slow pressurization (50s), and Fig. 4 and 6 that depict rapid inflation (2s).

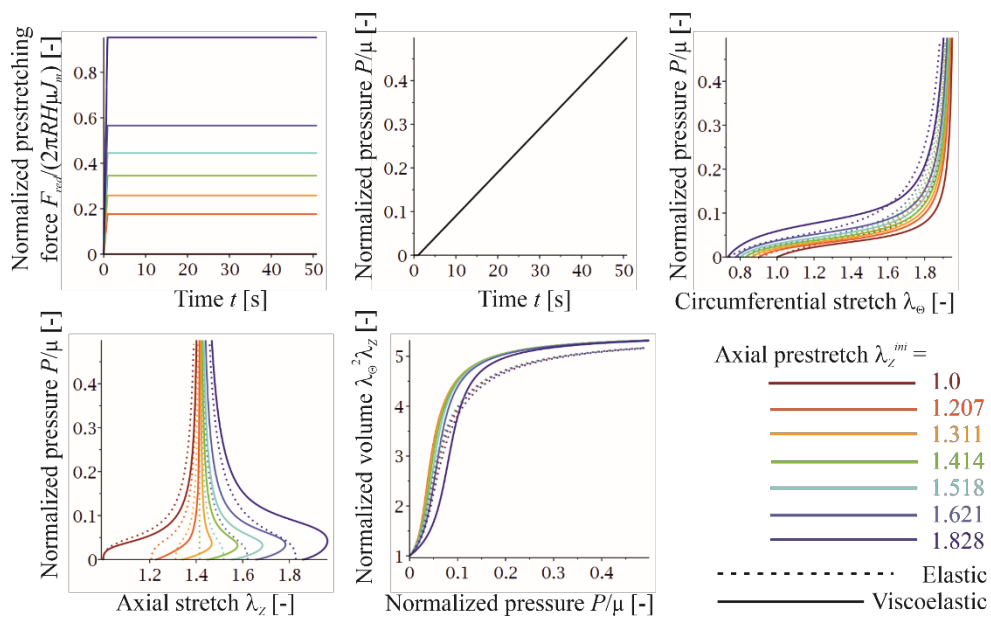


Figure 3. Closed tube within slow pressurization (50 s). Axial prestretching is induced by gradual increasing F_{red} under $P = 0$ and in the following pressurization F_{red} is held constant.

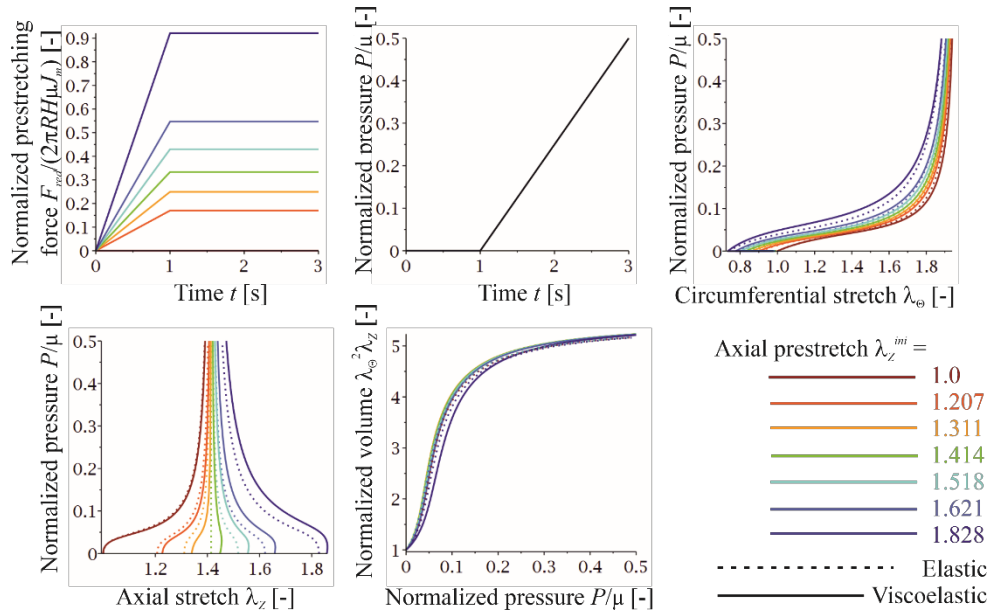


Figure 4. Closed tube within rapid pressurization (2 s). Axial prestretching is induced by gradual increasing F_{red} under $P = 0$ and in the following pressurization F_{red} is held constant.

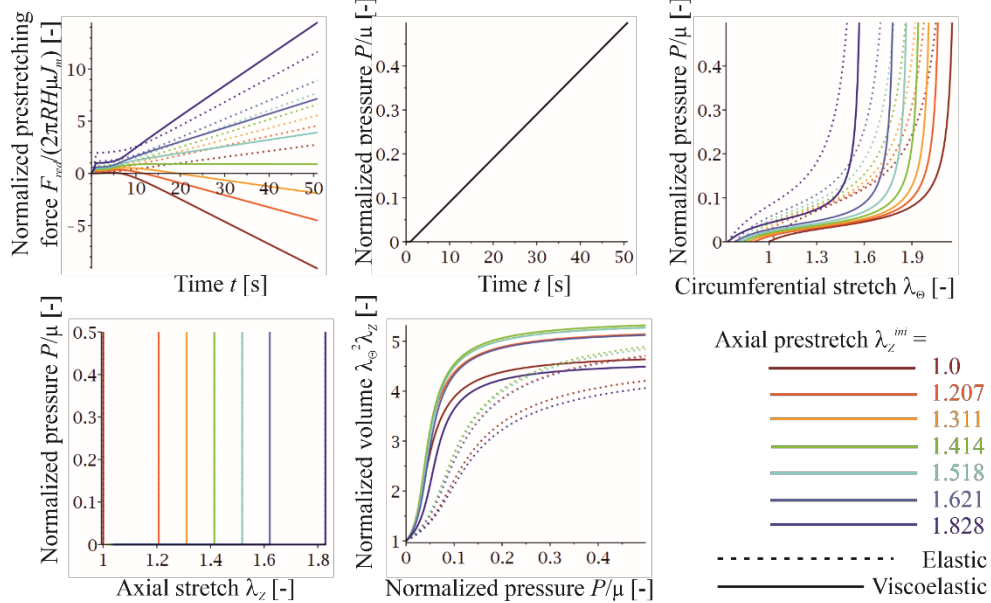


Figure 5. Open tube within slow pressurization (50 s). Axial prestretching is induced by gradual increasing of λ_z which is held constant, $\lambda_z = \lambda_z^{ini}$, during subsequent pressurization.

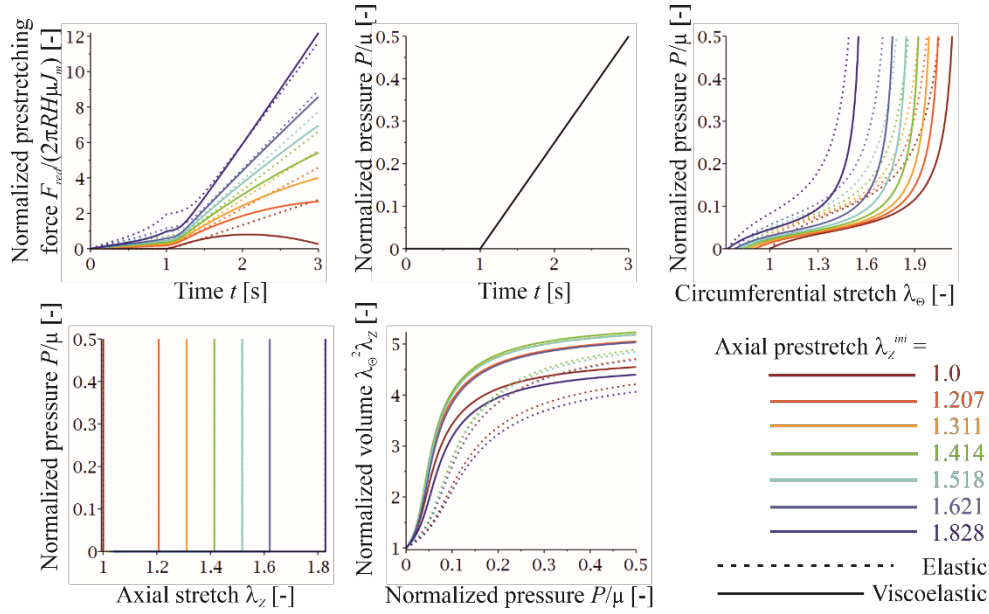


Figure 6. Open tube within rapid pressurization (2 s). Axial prestretching is induced by the gradual increasing of λ_z which is held constant, $\lambda_z = \lambda_z^{ini}$, during subsequent pressurization.

The different time courses of $F_{red}(t)$ make it easy to recognize what kind of boundary condition was applied. Note that the closed tube formulation implies $F_{red} = constant$ within the pressurization (see Fig. 3 and 4), whereas the open tube formulation, which necessitates preserving the tube length by some kinematical bond, leads to F_{red} varying during the pressurization (Fig. 5 and 6).

4. 1 Loss of monotony and inversion in axial response.

The closed tube exhibits significant differences in the axial deformation when the responses of the Gent (elastic) and QLV-Gent (viscoelastic) materials are compared. P - λ_z panels in Fig. 3 and 4 clearly show that the transition from elastic (dotted) to viscoelastic (solid) behavior is accompanied by a loss of monotony and that the non-monotonous response $\lambda_z(P)$ cannot preserve the inversion property in the axial deformation.

The analytical solution (24) gives for $J_m = 3$ the inversion in axial deformation at $\lambda_z^{ini} = \sqrt{2}$. This is depicted in Fig. 3 and 4 by a light green dotted line. This line divides the elastic responses into the pressure-induced elongation area (on the left) and the pressure-induced shortening area (on the right). On the contrary, in the viscoelastic model presented in Fig. 3, the light orange curve corresponding to $\lambda_z^{ini} = 1.311$ exhibits non-monotonous behavior and $\lambda_z^{ini} = 1.414, 1.518, 1.621,$ and 1.828 curves show it even more clearly.

However, mutual comparison of the solid curves in Fig. 3 and Fig. 4 suggests that the intensity of the loss of monotony is linked to how strong the viscoelastic effects (creep, relaxation) are. Both figures show results for the same tube (geometry and constitutive model) loaded with a pressure and force of the same magnitude, but at different loading speeds. The pressurization in Fig. 3 is 25 times slower than in Fig. 4. This can be interpreted as the viscoelastic effects in the material of the tube in Fig. 3 has 25 times longer time to take place. It is clearly visible when one compares red or dark blue solid curves in Fig. 3 and 4 and considers their distances from elastic solutions.

Since the open tube is held in its axial position by a kinematical bond, its axial deformation does not vary during pressurization (see P - λ_Z panels in Fig. 5 and 6). In this case, a more notable behavior shows a reduced axial force that represents the reaction in the kinematical bond. The solid curves in Fig. 5 and 6 show that $F_{red}(t)$ also loses its monotony, which can be considered as the reciprocal phenomenon to non-monotony in the axial deformation of the QLV-Gent tube held at a constant force.

Other viscoelastic effects that should be remarked upon are the different positions of λ_Z^{ini} in the elastic and viscoelastic responses of the closed tube (Fig. 3 and 4). This is the consequence of the chosen approach in which equal magnitudes of the prestretching force F_{red} were applied. Note that in all cases viscoelastic λ_Z^{ini} is on the right side of elastic λ_Z^{ini} which can be attributed to the creep that occurs during the initial elongation.

4.2 Preserving optimal volume property.

It has been shown in (Horný et al., 2014) that an axially prestretched abdominal aorta is more easily radially distensible than its non-prestretched counterpart. Horný and Netušil (2016) have shown how this property can be attributed to material and geometrical nonlinearity. In the recent work (Horný and Petřivý, 2020), we have shown how the inversion in axial deformation and the maximization of inflated volume are mutually associated. All these analyses have been carried out for elastic tubes and in the present study our attention is turned to the differences between elastic and viscoelastic models. Since hereditary integrals significantly complicate analytical treatment, numerical simulations are conducted to show whether axial prestretching can optimize the internal volume of the pressurized tube. The results suggest that the answer is positive. In other words, data suggests that there is a certain value of the prestretch at which a QLV-Gent tube attains maximal volume.

Volume–pressure responses obtained for the open tube in Fig. 5 and 6 show that the maximal normalized volume $v = \lambda_\phi^2 \lambda_Z$ is attained for the QLV-Gent material at the same axial prestretching λ_Z^{ini} as for the Gent material. This means $\lambda_Z^{ini} = \sqrt{1 + \frac{1}{3}J_m}$, which in our specific case, when $J_m = 3$, is $\lambda_Z^{ini} = \sqrt{2}$. Numerical simulations showed this result independently of the applied loading rate.

In the case of the closed tube, numerical results suggest that the axial prestretching at which maximal volume is attained depends on the loading rate. Axial prestretching corresponding to maximal volume was $\lambda_Z^{ini} = 1.207$ in the case of slow pressurization (50s), and $\lambda_Z^{ini} = 1.311$ in the case of rapid pressurization (2s). There is a property which connects these responses. As Fig. 3 and 4 show, they represent the maximal value of the axial prestretching at which monotonous axial deformation is obtained (within predefined values given by assignment in our analysis). This leads us to a generalization that can be expressed by the hypothesis that the maximal volume of the closed QLV-Gent tube is attained when the maximal λ_Z^{ini} , such that axial deformation obtained in the subsequent pressurization is monotonous, is used. We carried out some other calculations with a refined selection of λ_Z^{ini} in comparison to the values used in Fig. 3 and 4. The results were in accordance with the formulated hypothesis. These calculations are not included in Fig. 3 and 4 because they would make the figures rather unclear and difficult to understand.

It is evident that whilst numerical simulations cannot replace analytical proof, and our statements about the maximization of inflated volume remain in the form of hypotheses, numerical simulations are sufficient to demonstrate that this property should attract some more theoretical, but mainly technical attention. Our results suggest that inflation volume optimization by axial prestretching is not a purely theoretical concept linked to a more or less unrealistic assumption of perfect elasticity, but that it may also occur in realistic models that consider materials with dissipation effects.

4.3 Limitations of the Gent model

The Gent model (5) has been shown to be a helpful instrument in the analysis of the many theoretical problems of nonlinear elasticity (Horgan and Saccomandi, 2002a, 2003; Kanner and Horgan, 2007; Marckmann and Verron, 2006). It is popular thanks to its simple formulation, which still preserves the large strain stiffening property. Examples of its use are to be found in soft tissue biomechanics, when an assumption of the material isotropy is accepted (Horný et al., 2013; Mihai et al., 2015; Zhang et al., 2016; Mangan and Destrade, 2015). The Gent model belongs to the class of so-called generalized neo-Hookean models that do not consider the dependence of the strain energy density function on I_2 . However, reservations regarding the generalized neo-Hookean models are on the increase in the literature (Destrade et al., 2017; Anssari-Benam et al., 2021). Several studies have shown that such models fail to describe the mechanical response of elastomers under very large strains (Destrade et al., 2017). At this point, it is worth noting that the stretch ratios $\lambda > 2$ are rather unusual in soft tissue biomechanics, nevertheless in the case of rubber the situation is somewhat different. For example, Treloar's data (Treloar, 1944) for uniaxial tension contains experimental points with $\lambda > 5$. There are also objections linked to the incapability of the generalized neo-Hookean models to describe normal stresses within the simple shear loading and axial forces in the modeling of the torsion of a rubber cylindrical bar (Horgan and Saccomandi, 1999; Anssari-Benam et al., 2021).

Despite the above mentioned criticism, our study is based on the Gent model, mainly for to the following reasons: First, our study is a continuation of previous works (Horný and Petřivý, 2020) and the concrete progress made here lies in the fact that, to the best of our knowledge, for the first time the inversion point in the axial deformation of a tube is studied within the context of the viscoelastic behavior. We have put a greater emphasis on the comparison between elastic and viscoelastic behavior than on the theoretical discussion of various strain energy density functions.

In Horný and Petřivý (2020), it has been shown that the Mooney-Rivlin model, the simplest model incorporating both I_1 and I_2 invariants, has the property of the inversion point. The Mooney-Rivlin model nevertheless fails to exhibit significant strain stiffening, which is technically very important in the context of industrial applications of rubber elasticity and in soft tissue biomechanics. Therefore Mooney-Rivlin is not a good candidate for our analysis. In such a situation, the Gent model continues to be the model of first choice, meeting both the requirement of the presence of the inversion point and the requirement of large strain stiffening.

$$W = c_{10}(I_1 - 3) + c_{20}(I_1 - 3)^2 + c_{30}(I_1 - 3)^3 \quad (25)$$

$$W = c_1 \left[\frac{1}{2}(I_1 - 3) + \frac{1}{20N}(I_1^2 - 3^2) + \frac{11}{1050N^2}(I_1^3 - 3^3) + \frac{19}{7000N^3}(I_1^4 - 3^4) + \frac{519}{673750N^4}(I_1^5 - 3^5) \right] \quad (26)$$

$$W = \frac{1}{2}c_1(I_1 - 3) + \frac{3}{2}c_2 \ln\left(\frac{I_2}{3}\right) \quad (27)$$

$$W = -\frac{\mu J_m}{2} \ln\left(1 - \frac{I_1 - 3}{J_m}\right) + \frac{3}{2}c_2 \ln\left(\frac{I_2}{3}\right) \quad (28)$$

$$W = \frac{1}{2}c_1(I_1 - 3) + \sqrt{3}c_2(\sqrt{I_2} - \sqrt{3}) \quad (29)$$

Let us finally note that with the help of the computer algebra system Maple, it is easy to show that neither the Yeoh (25), nor the Arruda-Boyce model approximation based on (26), and neither examples of the models incorporating I_2 such as Gent-Thomas (27), Gent-Gent (28), and Carroll (29), show roots of (24) independent of λ_0 . This excludes them as models which allow for the inversion line in the pressure-axial deformation response of the pressurized tube and thus they are also not suitable for the purposes of our study. For the sake of completeness, let us add that in all the aforementioned equations, I_1 and I_2 are defined according to (2) and c_{10} , c_{20} , c_{30} , c_1 , c_2 , and N are material parameters.

5. Conclusion

Previous studies have shown that axial prestretching significantly improves the capability of the radial distension of pressurized tubes (Horný et al., 2014; Horný and Netušil, 2016). It was also shown that there are material models in which axial deformation represents the way an inflation volume reached at a given pressure can be optimized (Horný and Petřivý, 2020). The present study shifts our attention from purely theoretical elastic models to a more realistic assumption of the viscoelastic behavior of a material. It has been shown that the QLV viscoelastic model used for thin-walled tubes, assuming the elastic part of the material response to be given by the Gent model, loses the property of the global inversion in axial deformation but still preserves the potential to optimize the inflation volume by means of axial prestretching. This result could be helpful in designing elastomer pipelines and pumps, and could also contribute to the understanding of the principals of blood circulation's physiology.

Acknowledgement

This study has been supported by the Czech Science Foundation in project 18-26041S entitled "Effect of axial prestretch on the mechanical response of nonlinearly elastic and viscoelastic tubes".

References

- Anssari-Benam, A., Bucchini, A., Saccomandi, G., 2021. On the central role of the invariant I2 in nonlinear elasticity. *International Journal of Engineering Science* 163. <https://doi.org/10.1016/j.ijengsci.2021.103486>
- Bergel, D.H., 1961. The static elastic properties of the arterial wall. *J. Physiol.* 156, 445-457. <https://doi.org/10.1113/jphysiol.1961.sp006686>.
- Bergström, J., 2015. *Mechanics of Solid Polymers: Theory and Computational Modeling*. Elsevier, Amsterdam.
- Brossollet, L.J., Vito, R.P., 1995. An alternate formulation of blood vessel mechanics and the meaning of the in vivo property. *J. Biomech.* 1995, 679-687. [https://doi.org/10.1016/0021-9290\(94\)00119-O](https://doi.org/10.1016/0021-9290(94)00119-O).
- Christensen, R.M., 1982. *Theory of Viscoelasticity: An Introduction*. Academic Press, Tokyo.
- De Pascalis, R., Abrahams, I.D., Parnell, W.J., 2014. On nonlinear viscoelastic deformations: A reappraisal of fung's quasi-linear viscoelastic model. *Proc. R. Soc. A Math. Phys. Eng. Sci.* 470: 20140058. <https://doi.org/10.1098/rspa.2014.0058>.
- De Pascalis, R., Parnell, W.J., Abrahams, I.D., Shearer, T., Daly, D.M., Grundy, D., 2018. The inflation of viscoelastic balloons and hollow viscera. *Proc. R. Soc. A Math. Phys. Eng. Sci.* 474:20180102. <https://doi.org/10.1098/rspa.2018.0102>.
- Destrade, M., Saccomandi, G., Sgura, I., 2017. Methodical fitting for mathematical models of rubber-like materials. *Proceedings of the Royal Society A: Mathematical, Physical and Engineering Sciences* 473. <https://doi.org/10.1098/rspa.2016.0811>
- Dobrin, P.B., Doyle, J.M., 1970. Vascular smooth muscle and the anisotropy of dog carotid artery. *Circ. Res.* 27, 105-119. <https://doi.org/10.1161/01.RES.27.1.105>.
- Dobrin, P.B., 1986. Biaxial anisotropy of dog carotid artery: Estimation of circumferential elastic modulus. *J. Biomech.* 19, 351-358. [https://doi.org/10.1016/0021-9290\(86\)90011-4](https://doi.org/10.1016/0021-9290(86)90011-4).

Manuscript version: Petřivý, Z., Horný, L. (2022) Effect of viscoelasticity on inversion in axial deformation and on the volume of pressurized thin-walled tubes. *European Journal of Mechanics - A/Solids*, 96, art. no. 104763. Publisher version is available via <https://doi.org/10.1016/j.euromechsol.2022.104763>

Dobrin, P.B., Schwarcz, T.H., Mrkvicka, R., 1990. Longitudinal retractive force in pressurized dog and human arteries. *J. Surg. Res.* 48, 116-120. [https://doi.org/10.1016/0022-4804\(90\)90202-D](https://doi.org/10.1016/0022-4804(90)90202-D).

Ferruzzi, J., Achille, P.D., Tellides, G., Humphrey, J.D., 2018. Combining in vivo and in vitro biomechanical data reveals key roles of perivascular tethering in central artery function. *PLoS. ONE*. 13: e0201379. <https://doi.org/10.1371/journal.pone.0201379>.

Fuchs, R.F., 1900. Zur Physiologie und Wachstumsmechanik des Blutgefäßsystems. *Archiv für Physiologie. Veit & Comp.*, pp. 102-154.

Fung, Y.C., 1981. *Biomechanics: Mechanical Properties of Living Tissues*. Springer Verlag, New York.

Gent, A.N., 1996. A New Constitutive Relation for Rubber. *Rubber Chem. Technol.* 69, 59-61. <https://doi.org/10.5254/1.3538357>.

Han, H.-C., Fung, Y.-C., 1995. Longitudinal strain of canine and porcine aortas. *J. Biomech.* 28, 637-641. [https://doi.org/10.1016/0021-9290\(94\)00091-H](https://doi.org/10.1016/0021-9290(94)00091-H).

Holzappel, G.A., 2000. *Nonlinear Solid Mechanics: A Continuum Approach for Engineering*. John Wiley and Sons, Chichester.

Horgan, C.O., Saccomandi, G., 1999. Simple Torsion of Isotropic, Hyperelastic, Incompressible Materials with Limiting Chain Extensibility. *Journal of Elasticity* 56, 159–170. <https://doi.org/10.1023/A:1007606909163>

Horgan, C.O., Saccomandi, G., 2002a. Constitutive Modelling of Rubber-Like and Biological Materials with Limiting Chain Extensibility. *Mathematics and Mechanics of Solids* 7, 353-371. <https://doi.org/10.1177/108128028477>

Horgan, C.O., Saccomandi, G., 2002b. A Molecular-Statistical Basis for the Gent Constitutive Model of Rubber Elasticity. *J. Elast.* 68, 167-176. <https://doi.org/10.1023/A:1026029111723>.

Horgan, C.O., Saccomandi, G., 2003. A description of arterial wall mechanics using limiting chain extensibility constitutive models. *Biomech. Model. Mechanobiol.* 1, 251-266. <https://doi.org/10.1007/s10237-002-0022-z>.

Horný, L., Adamek, T., Gultova, E., Zitný, R., Vesely, J., Chlup, H., Konvickova, S., 2011. Correlations between age, prestrain, diameter and atherosclerosis in the male abdominal aorta. *J. Mech. Behav. Biomed. Mater.* 4: 2128-2132. <https://doi.org/10.1016/j.jmbbm.2011.07.011>.

Horný, L., Adamek, T., Kulvajtova, M., 2014. Analysis of axial prestretch in the abdominal aorta with reference to post mortem interval and degree of atherosclerosis. *J. Mech. Behav. Biomed. Mater.* 33: 93-98. <https://doi.org/10.1016/j.jmbbm.2013.01.033>.

Horný, L., Adámek, T., Kulvajtová, M., 2017. A comparison of age-related changes in axial prestretch in human carotid arteries and in human abdominal aorta. *Biomech. Model. Mechanobiol.* 16, 375-383. <https://doi.org/10.1007/s10237-016-0797-y>.

Horný, L., Adamek, T., Zitny, R., 2013. Age-Related Changes in Longitudinal Prestress in Human Abdominal Aorta. *Arch. Appl. Mech.* 83, 875-888. <https://doi.org/10.1007/s00419-012-0723-4>.

Horný, L., Netušil, M., 2016. How does axial prestretching change the mechanical response of nonlinearly elastic incompressible thin-walled tubes. *Int. J. Mech. Sci.* 106, 95-106. <https://doi.org/10.1016/j.ijmecsci.2015.08.014>.

Manuscript version: Petřivý, Z., Horný, L. (2022) Effect of viscoelasticity on inversion in axial deformation and on the volume of pressurized thin-walled tubes. *European Journal of Mechanics - A/Solids*, 96, art. no. 104763. Publisher version is available via <https://doi.org/10.1016/j.euromechsol.2022.104763>

Horný, L., Netušil, M., Voňavková, T., 2014. Axial prestretch and circumferential distensibility in biomechanics of abdominal aorta. *Biomech. Model. Mechanobiol.* 13, 783-799. <https://doi.org/10.1007/s10237-013-0534-8>.

Horný, L., Petřivý, Z., 2020. Inversion point and internal volume of pressurized nonlinearly elastic tube. *Int. J. Non. Linear. Mech.* 125:103530. <https://doi.org/10.1016/j.ijnonlinmec.2020.103530>.

Humphrey J.D., 2002. *Cardiovascular Solid Mechanics: Cells, Tissues, and Organs*. Springer-Verlag, New York.

Humphrey, J.D., Eberth, J.F., Dye, W.W., Gleason, R.L., 2009. Fundamental role of axial stress in compensatory adaptations by arteries. *J. Biomech.*, 1-8. <https://doi.org/10.1016/j.jbiomech.2008.11.011>.

Jha, N.K., Reinoso, J., Dehghani, H., Merodio, J., 2019. Constitutive modeling framework for residually stressed viscoelastic solids at finite strains. *Mechanics Research Communications* 95, 79-84. <https://doi.org/10.1016/j.mechrescom.2019.01.003>

Kamenskiy, A., Seas, A., Bowen, G., Deegan, P., Desyatova, A., Bohlim, N., Poulson, W., Mactaggart, J., 2016. In situ longitudinal pre-stretch in the human femoropopliteal artery. *Acta Biomater.* 32, 231-237. <https://doi.org/10.1016/j.actbio.2016.01.002>.

Kanner, L.M., Horgan, C.O., 2007. Elastic Instabilities for Strain-Stiffening Rubber-Like Spherical and Cylindrical Thin Shells Under Inflation. *Int. J. Non-Lin. Mech.* 45, 204-215. <https://doi.org/10.1016/j.ijnonlinmec.2006.10.010>.

Kratochvíl, O., Chlup, H., Horný, L., Špaček, M., Měříčka, P., 2020. Inflation-extension behaviour of the human vena saphena magna, in: Fusek, M., Cienciala, J., Kořínek, M., Machalla, V., Šmach, J., editors. *Experimental Stress Analysis 2020*, Ostrava: VŠB – Technical University of Ostrava, pp. 248-251.

Mangan, R., Destrade, M., 2015. Gent models for the inflation of spherical balloons. *Int. J. Non Linear. Mech.* 68, 52-58. <https://doi.org/10.1016/j.ijnonlinmec.2014.05.016>.

Marckmann, G., Verron, E., 2006. Comparison of Hyperelastic Models for Rubber-Like Materials. *Rubber Chem. Technol.* 79, 835-858. <http://doi.org/10.5254/1.3547969>.

Merodio, J., Ogden R.W. (Eds.), 2020. *Constitutive Modelling of Solid Continua*. Springer, Cham.

Merodio, J., Rajagopal, K.R., 2007. On Constitutive Equations For Anisotropic Nonlinearly Viscoelastic Solids. *Mathematics and Mechanics of Solids* 12, 131-147. <https://doi.org/10.1177/1081286505055472>

Mihai, L.A., Chin, L., Janmey, P.A., Goriely, A., 2015. A comparison of hyperelastic constitutive models applicable to brain and fat tissues. *J. R. Soc. Interface*, 12:20150486. <https://doi.org/10.1098/rsif.2015.0486>.

Ogden, R.W., Saccomandi, G., 2007. Introducing mesoscopic information into constitutive equations for arterial walls. *Biomech. Model. Mechanobiol.* 6, 333-344. <https://doi.org/10.1007/s10237-006-0064-8>.

Ogden, R.W., Schulze-Bauer, C.A.J., 2000. Phenomenological and structural aspects of the mechanical response of arteries, in: Casey J, Bao G, editors. *Mechanics in Biology*, American Society of Mechanical Engineers, Applied Mechanics Division vol. 242, New York, pp. 125-140.

Manuscript version: Petřivý, Z., Horný, L. (2022) Effect of viscoelasticity on inversion in axial deformation and on the volume of pressurized thin-walled tubes. *European Journal of Mechanics - A/Solids*, 96, art. no. 104763. Publisher version is available via <https://doi.org/10.1016/j.euromechsol.2022.104763>

Patel, D.J., Fry, D.L., 1966. Longitudinal tethering of arteries in dogs. *Circ. Res.* 19, 1011-1021. <https://doi.org/10.1161/01.RES.19.6.1011>.

Schulze-Bauer, C.A.J., Mörth, C., Holzapfel, G.A., 2003. Passive biaxial mechanical response of aged human iliac arteries. *J. Biomech. Eng.* 125, 395-406. <https://doi.org/10.1115/1.1574331>.

Sommer, G., Benedikt, C., Niestrawska, J.A., Hohenberger, G., Viertler, C., Regitnig, P., Cohnert, T.U., Holzapfel, G.A., 2018. Mechanical response of human subclavian and iliac arteries to extension, inflation and torsion. *Acta Biomater.* 75, 235-252. <https://doi.org/10.1016/j.actbio.2018.05.043>.

Sommer, G., Regitnig, P., Køltringer, L., Holzapfel, G.A., 2010. Biaxial mechanical properties of intact and layer-dissected human carotid arteries at physiological and supraphysiological loadings. *Am. J. Physiol. Heart Circ. Physiol.* 298, 898-912. <https://doi.org/10.1152/ajpheart.00378.2009>.

Takamizawa, K., Hayashi, K., 1987. Strain energy density function and uniform strain hypothesis for arterial mechanics. *J. Biomech.* 20, 7-17. [https://doi.org/10.1016/0021-9290\(87\)90262-4](https://doi.org/10.1016/0021-9290(87)90262-4).

Treloar, L.R.G., 1944. Stress-strain data for vulcanised rubber under various types of deformation. *Transactions of the Faraday Society* 40. <https://doi.org/10.1039/TF9444000059>

Van Loon, P., Klip, W., Bradley, E.L., 1977. Length-force and volume-pressure relationships of arteries. *Biorheology.* 14, 181-201. <https://doi.org/10.3233/BIR-1977-14405>.

Weizsäcker, H.W., Lambert, H., Pascale, K., 1983. Analysis of the passive mechanical properties of rat carotid arteries. *J. Biomech.* 16, 703-715. [https://doi.org/10.1016/0021-9290\(83\)90080-5](https://doi.org/10.1016/0021-9290(83)90080-5).

Wineman, A., 2020. Viscoelastic solids, in: Merodio, J., Ogden, R., editors. *Constitutive Modelling of Solid Continua*, Cahm: Springer, pp. 81-124.

Zhang, W., Sommer, G., Niestrawska, J.A., Holzapfel, G.A., Nordsletten, D., 2022. The effects of viscoelasticity on residual strain in aortic soft tissues. *Acta Biomaterialia* 140, 398-411. <https://doi.org/10.1016/j.actbio.2021.11.019>

Zhang, W., Zhang, R.R., Feng, L.L., Li, Y., Wu, F., Wu, C.W., 2016. Mechanical response of brain stem in compression and the differential scanning calorimetry and FTIR analyses. *J. Appl. Mech. Trans. ASME.* 83:091005. <https://doi.org/10.1115/1.4033890>.

Zhou, L., Wang, S., Li, L., Fu, Y., 2018. An evaluation of the gent and gent-gent material models using inflation of a plane membrane. *Int. J. Mech. Sci.* 146-147, 39-48. <https://doi.org/10.1016/j.ijmecsci.2018.07.035>.